Int J Adv Manuf Technol (2012) 59:859–867
DOI 10.1007/s00170-011-3556-3

ORIGINAL ARTICLE

# A flexure-based long-stroke fast tool servo for diamond turning

**Qiang Liu · Xiaoqin Zhou · Pengzi Xu · Qing Zou · Chao Lin**

Received: 22 December 2010 / Accepted: 31 July 2011 / Published online: 18 August 2011


**Abstract** This paper describes the development of the fast tool servo (FTS) in detail and categorizes existing FTSs according to different principles. The characteristics and differences of these FTSs have been analyzed. A flexure-based long-stroke FTS system for diamond turning is presented with displacement range of 1 mm and bandwidths of 10 Hz. The vertical jump is about 0.045 μm, and the full stroke tracking error is less than 0.15%. A voice coil motor and a piezoelectric actuator are used as the driving elements, and two flexure hinges are developed as the guide mechanisms. The FTS utilizes a linear encoder and a capacitive sensor to measure the displacement of the tool for closed-loop control. The electromechanical design of the FTS and its motion analysis are described. Experimental tests have been carried out to verify the performance of the FTS system. This long-stroke FTS has the advantage of easy machining, high resonance frequency, and error compensation in *y*-axis direction.

**Keywords** Fast tool servo · Diamond turning · Voice coil motor · Piezoelectric actuator · Flexure hinge

| | |
|---|---|
| FTS | Fast tool servo |
| LLNL | Lawrence Livermore National Laboratory |
| MIT | Massachusetts Institute of Technology |
| GIT | Georgia Institute of Technology |
| VCM | Voice coil motor |
| PID | Proportional integral derivative |

Q. Liu · X. Zhou (✉) · P. Xu · Q. Zou
School of Mechanical Science and Engineering, Jilin University, Changchun, China
e-mail: xqzhou@jlu.edu.cn

C. Lin
Space Optics Research Laboratory, Changchun Institute of Optics, Fine Mechanics and Physics, Chinese Academy of Sciences, Changchun, China

## 1 Introduction

Diamond turning using a fast tool servo (FTS) is the most popular technique which can compensate the motion errors of diamond-turning machines [1–4] or produce freeform optical surfaces [5–8]. The working principle of FTS is shown in Fig. 1. Workpiece is clamped on the spindle; FTS is fixed on the slide of the machine which can move along *z*-axis direction. According to the concave–convex properties of the workpiece, FTS translates the cutting tool in and out of the workpiece several times per revolution to obtain a complex surface. The FTSs working frequency is integer multiple of the spindle rotational frequency.

The FTS system mainly contains five parts: cutting tool, actuator, guide mechanism, feedback sensor, and controller. The main differences of FTSs are reflected in the actuators and guide mechanisms. Based on working principles, the actuators of FTSs can be categorized in four types: piezoelectric actuators, magnetostrictive actuators, Lorentz force motors, and normal-stress electromagnetically driven actuators [9]. Mainly two types of guide mechanisms are used in FTSs: air bearings and flexure hinges. FTSs can also be categorized according to their operating range, frequency, or motion mode. Short stroke is defined as less than 100 μm, intermediate stroke as between 100 μm and 1 mm, and long stroke as above 1 mm [10, 11]. According to motion mode, there are two types: rotary FTS and linear FTS. In the design of FTS, the actuator and guide mechanism are selected based on the need of FTSs' operating stroke, frequency, and motion mode.

### 1.1 The development of FTSs

FTS first appeared in LLNL in 1980s; Patterson designed a micro-feed system for error compensation [1]. Then, MIT, GIT, Tohoku University, Precitech, Moore Nanotechnology, and many other units have developed

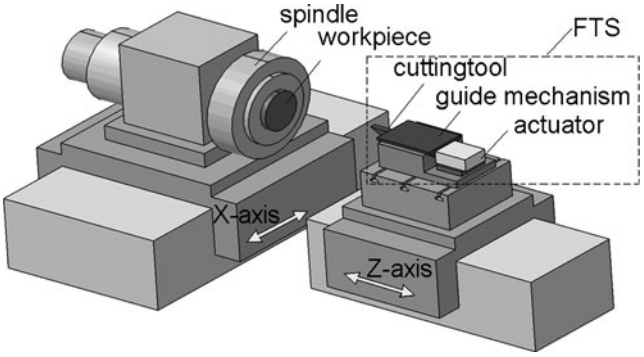


**Fig. 1** Working principle of FTS

many FTSs with different drivers and structures. Trumper from MIT did a lot in the study of FTS. His student Ludwick analyzed the advantages and disadvantages of linear FTS and rotary FTS in his doctoral dissertation [7]. He pointed out that the rotary FTS can be designed to transmit essentially zero reaction forces into the machine base and achieve higher accelerations at the tool tip. In his dissertation, he developed a rotary FTS with a rotary motor and bearings with peak accelerations of 500 m/s$^2$. This FTS can machine 100 mm diameter parts having feature amplitudes of up to 3 cm with micron-level form error. He also described that rotary FTSs caused a parasitic lateral displacement on the tool tip and had some difficulties in toolpath generation.

Richard's dissertation had an extensive literature review on existing fast tool servo before 2005 [10] and designed two FTSs which reduced the lateral displacement. One was actuated by a rotary motor: −3 dB bandwidth of 2 kHz, maximum tool travel of 50 μm PP; the other was driven by a hybrid rotary/linear electromagnetic actuator: −3 dB bandwidth of 10 kHz, maximum tool travel of 70 μm PP. Lu described the performances of existing FTS actuators based on the working principle in his dissertation in 2005 [9]. The dissertation came to a conclusion that Lorentz FTSs have longer strokes but lower bandwidths than other FTSs. Besides, the stroke and the bandwidth are two separate performance parameters which cannot be achieved simultaneously for most cases. He designed a short-stroke FTS actuated by a normal-stress electromagnetically driven actuator with 23 kHz closed-loop bandwidth, as low as 1.7 nm RMS error and 30 μm stroke.

It can be gotten that: magnetostrictive actuators are still in the development stage and the existing FTSs are not satisfactory. Piezoelectric actuators and Lorentz force motors have been fully developed. The former have been widely used in short-stroke and intermediate-stroke FTSs. Lorentz force motors are suitable for long-stroke FTSs with lower working frequency. Because of the difficulty of controlling in the presence of inherent nonlinearities, FTSs actuated by normal-stress electromagnetically driven actuators are only suitable for special requirements which need ultra-high frequency and short stroke.

From 2005 until now, more academic institutions have been paying attention to FTSs, and a lot of FTSs have appeared. Most of these are short-stroke FTSs utilizing piezoelectric actuators and flexure hinges [12–17]. A few of intermediate-stroke and long-stroke FTSs also have been developed. Kim developed an intermediate-stroke FTS with a piezoelectric actuator, flexure hinges, and mechanical levers [18]. Noh designed a FTS for micro-lens fabrication, which was actuated by a VCM with a disk spring [19].

Air bearings have been used for long-stroke FTSs. Buescher [11] developed a long-stroke FTS utilizing a linear motor and an air bearing. This FTS was designed to machine non-rotationally symmetric surfaces with sag of ±2 mm at 20 Hz. But there was vertical vibration with amplitude of 0.2 μm. Zdanowicz developed a new system to address the limitation of Buescher's FTS with VCM and air bearing [20]. Marten developed a long-stroke fast tool servo which consisted of an air bearing stage and a three-phase oil-cooled linear motor. The linear FTS had a stroke of 25 mm and was capable of getting acceleration of 100 m/s$^2$ [21]. Precitech [22] and Moore Nanotechnology [23] developed several FTSs with air bearings and VCMs. However, the high-precision air bearing is difficult to machine and install. An air supply system has to be provided for the air bearing. Besides, the air bearing has a low damping that a damping structure must be designed for FTS. The flexure hinge, which is simple in structure and fabrication, can also obtain high guide accuracy. Rakuff [24, 25] developed a long-stroke FTS with a VCM and a flexure hinge which had maximum accelerations of 260 m/s$^2$ and bandwidths of up to 140 Hz. The maximum displacement range of the cutting tool was 2 mm. But the disadvantage of this FTS is that the flexure structure has a low resonant frequency which can cause resonance easily and low stiffness in the $y$-axis direction liable to generate vertical vibration. All of these have an adverse impact on the workpiece surface quality.

Then, this paper has come to the conclusion that: (1) short-stroke FTSs are usually actuated by piezoelectric drivers and guided by flexure hinge structures which are more suitable for error compensation; (2) both piezoelectric actuator and VCM can be used in intermediate stroke FTSs but FTSs actuated by piezoelectric actuators often have a low resonance frequency because of the lever mechanism. The lever mechanisms also bring hysteresis and tracking error because of the lever bending; (3) long-stroke FTSs use VCMs or rotary motors as the actuating elements and air bearings as the guide mechanisms. However, there are several disadvantages of air bearing used for FTS.

So, a long-stroke FTS with a VCM and a high performance flexure hinge is the best choice for diamond turning of freeform optics.

### 1.2 Research content of this study

In the freeform surfaces diamond-turning process, both the horizontal and vertical directions are error-sensitive directions [18, 26]. The tool position errors in the two directions will bring form errors to the workpiece.

FTSs usually have vertical vibrations because of the cutting force or other reasons during the cutting process. In this study, a new long-stroke FTS has been developed which can compensate the vertical direction errors. It used a VCM and a piezoelectric actuator as the driving elements. Two parallelogram flexure mechanisms were designed as the translation slides of the FTS. This FTS can provide a high resonance frequency in $z$-axis direction and high stiffness in $y$-axis direction. The prototype FTS was mounted and tested on a test bed. A linear encoder and a capacitive sensor were used as feedback sensors. In order to obtain an optimal performance of the system, a closed-loop control system with PID controller was implemented and tested.

The remainder of this paper is organized as follows. In the second part, the electromechanical design of the FTS is illustrated. Next, we analyze the motion characteristic of the flexure hinge system, and the open-loop control performances are tested. Then, closed-loop control experimental tests have been carried out to verify the performance of the FTS. Lastly, the conclusion of this paper is drawn.

## 2 FTS electromechanical design

The actuator of the FTS must have enough force. It should enable a very fast tool motion at the diamond tool tip and provide enough cutting force. To ensure the accuracy of the diamond turning, the resonance frequency of the guide mechanism in the tool's infeed direction and the stiffness in the vertical direction should be as high as possible.

### 2.1 Flexure hinge

The large deformation of flexure hinge will bring down the resonance frequency and stiffness. Furthermore, the cutting vibration caused by the periodic variation of cutting force has an adverse effect on the freeform surfaces diamond turning. So, long-stroke FTSs are usually guided by air bearings.

In this study, a new long-stroke flexure mechanism has been developed which has a high stiffness and high resonance frequency. As shown in Fig. 2, the flexure hinge contains two parts: the long-stroke flexure hinge to achieve $z$-axis direction stroke and the short-stroke flexure hinge compensating the $y$-axis direction displacement. The long-stroke flexure hinge consists of eight circular notch-type hinges, four links, and two bottoms. The down bottom is fixed, and the up bottom can move along $z$-axis direction. According to the characteristics of the parallelogram, when the up bottom moves in the $z$-axis direction, it still produces vertical displacement ($y$-axis direction). The short-stroke flexure hinge with parallelogram structure can offset this additional displacement. The two parallelogram structure hinges can make sure that the angle of the tool cutting face cannot be changed during cutting. Heat-treated 17Cr–4Ni stainless steel was chosen as the material. The photo of the new FTS is shown in Fig. 3.

The dimensions of the parallel notch hinges are determined through the formulae of bending stiffness $K_B$ given by Paros and Weisbord [27] as follows:

$$K_B = \frac{2Edt^{5/2}}{9\pi R^{1/2}} \tag{1}$$

where $R$ is the notch radius, $t$ is the thickness, $d$ is the width of the notch hinge, and $E$ is the Young's Modulus of flexure materials. According to the law of energy conservation, the following equation can be obtained:

$$Fx = \frac{1}{2}K_B\alpha^2 \tag{2}$$

where $F$ is the force given on the flexure hinge, $x$ is the displacement generated by $F$, and $\alpha$ is the rotational angle of flexure hinge. For the long-stroke flexure hinge, $\alpha_1$ can be approximately equal to $z/L_1$, and the short-stroke flexure hinge $\alpha_2=\Delta y/L_2$. So, the $z$-axis direction stiffness of the long-stroke flexure hinge can be obtained using the following equation:

$$K_1 = \frac{F_1}{z} = \frac{4K_{B1}}{L_1^2} \tag{3}$$

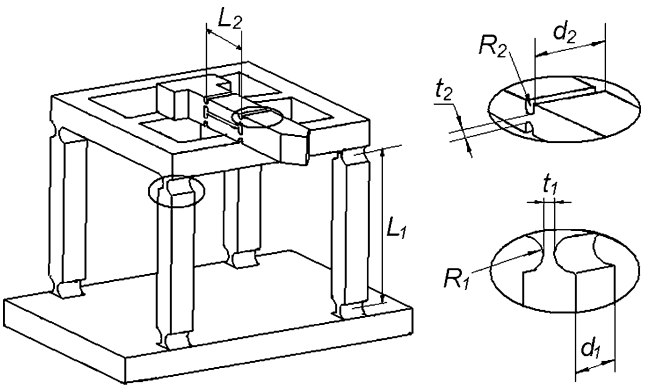


**Fig. 2** View of the flexure structure

**Fig. 3** Photo of the long-stroke FTS

where $K_{B1} = \frac{2Ed_1t_1^{5/2}}{9\pi R_1^{1/2}}$ is the bending stiffness of the long-stroke flexure hinge and $L_1$ is the length of the two circular notch-type hinges. The other parameters are shown in Fig. 1.

The $y$-axis stiffness of the short-stroke flexure hinge can be obtained by:

$$K_2 = \frac{F_2}{\Delta y} = \frac{2K_{B2}}{L_2^2} \tag{4}$$

where, $K_{B2} = \frac{2Ed_2t_2^{5/2}}{9\pi R_2^{1/2}}$ is the bending stiffness of the short-stroke flexure hinge, $L_2$ is the distance between the two circular notch-type hinges. Other parameters can be seen in Fig. 1.

The characteristics such as mass, spring constant, and other coefficients of the developed flexure structure are given in Table 1. $M_1$ contains the mass of the coil assemble of the VCM, the moving part of the long-stroke flexure hinge, the short-stroke flexure hinge, and screws.

### 2.2 The encoder and actuator of the FTS

A BEI Kimco VCM was used to drive the long-stroke flexure hinge. This actuator provides maximum continuous stall forces of 82.74 N (18.6 lbs) and short-term peak forces of 266.89 N (60 lbs). The mass of the moving parts is about 230 g. During work, because of the moving part of the motor fixed on the up bottom of the long-stroke flexure hinge, the motion of FTS will cause motor output force error. But the error can be ignored. The short-stroke flexure hinge was driven by a piezoelectric actuator with axial stiffness of 100 N/μm and maximum output force of 1,750 N. The piezoelectric actuator was installed on the up bottom of the long-stroke flexure hinge, which can drive the short-stroke flexure hinge to move along $y$-axis direction. The piezoelectric actuator was preloaded by wedges. The actuator provides a stroke of 15 μm with size of 7×7×18 mm which is small enough for the installation.

The long stroke was measured by a Renishaw linear encoder with the resolution of 0.01 μm. The maximum speed of the encoder can reach up to 270 mm/s. The linearity of the scale is about ±3 μm/m. The read head was installed on the case of the FTS, and the scale was pasted on the up bottom. The gap between the scale and the read head is cyclically changing because of the up bottom movement. But, the gap changes are small enough not to affect the feedback accuracy. A capacitive sensor was chosen as the feedback sensor of the short-stroke flexure hinge. The resolution is 0.0077% of the full stroke and working bandwidth is up to 35 kHz, with an effective measurement range of 200 μm. The probe was fixed on the up case of the FTS, which can obtain the movement of the tool in the $y$-axis direction.

**Table 1** The main results of the optimal design

| Parameters | Value | Parameters | Value |
|---|---|---|---|
| $t_1$ | 1 mm | $t_2$ | 1 mm |
| $d_1$ | 10 mm | $d_2$ | 10 mm |
| $R_1$ | 4 mm | $R_2$ | 1 mm |
| $L_1$ | 60 mm | $L_2$ | 20 mm |
| $K_1$ | 75.49 N/mm | $K_2$ | 0.68 N/μm |
| $M_1$ | 640 g | $M_2$ | 40 g |

## 3 Motion analysis and open-loop performance test of FTS

Because of the long stroke and the large mass of the moving part, the inertia force is very large to affect the tracking accuracy of the tool when the long-stroke FTS works at a high frequency. Until now, this problem is solved by balancing mechanism [20, 21, 24, 25]. This would increase the costs and the size of the FTSs and bring great difficulty in closed-loop control. In this study, the maximum inertia force is about 1.26 N when the FTS works at 10 Hz. According to reference [20], the effect on machining process generated by this force can be neglected.

### 3.1 Motion analysis

As shown in Fig. 4, when given a drive force $F_1$, the up bottom of the long-stroke flexure hinge will generate displacement $z$ in the $z$-axis direction and $\Delta y$ in the $y$-axis direction. At the same time, the piezoelectric actuator drives the short-stroke flexure to generate displacement $\Delta y$ to offset the vertical displacement generated by the long-

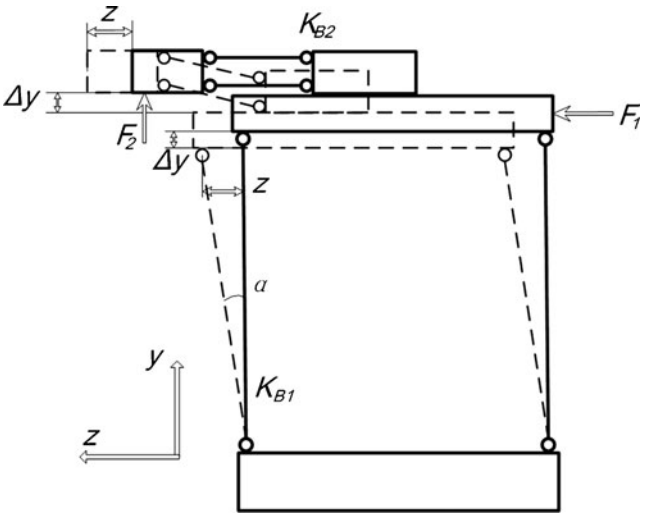


**Fig. 4** Working principle of the new FTS

stroke flexure. The relationship between $\Delta y$ and $z$ is determined by the following equation:

$$\Delta y = L_1 - \sqrt{L_1^2 - z^2} \tag{5}$$

When the diamond tool has a stroke of 0.5 mm in $z$-axis direction, $\Delta y$ reaches its maximum value of about 2.1 μm. There may be manufacturing errors of the flexure hinge and other errors which can enlarge the vertical displacement $\Delta y$. So, the actual displacement of the short-stroke flexure hinge during the cutting process will contain two parts: $\Delta y$ and other vertical displacement generated by cutting force or other factors. So, the short-stroke flexure hinge should have a stroke much longer than 2.1 μm.

## 3.2 Open-loop control tests

The open-loop control experiments were carried out to test the performance of the flexure mechanism system. The stiffness of the flexure system was tested to be 74.76 N/mm in the $z$-axis direction, which is near the calculation value. The $y$-axis direction stiffness is 8.9 N/μm.

### *3.2.1 Impact test*

The damping coefficient of the structure is determined through an impact test on the structure using the following equation:

$$D = 2\xi\sqrt{K \cdot M} \tag{6}$$

where $M$ is mass of flexure structure and $\xi$ is the damping ratio which is given by $\xi = 1/\left[2j\pi \ln\left(x_i/x_{i+j}\right)\right]$, $x_i$ and $x_j$ is the amplitude from the impact response curve. So, the damping coefficient of the large stroke flexure is 25.25 Ns/m. According to the FFT of the impact response, the first-order resonance frequency is approximately 109.6 Hz, which is far larger than the FTS working frequency.

### *3.2.2 Open-loop control test of the piezoelectric actuator*

The hysteresis loop of the piezoelectric actuator driving flexure-based mechanism under open loop control is shown in Fig. 5. The lower curve represents the expansion process and the upper curve represents the retraction process. When a 100-V control signal was applied to the piezoelectric actuator, the maximum displacement of the flexure-based mechanism was approximately 14.7 μm. It is noted that when the displacement curve of the expansion process is different from that of retraction process, this is the hysteresis effect. The maximum difference approximately reaches 1.1 μm which is not allowed in the precision and ultra-precision turning.

### *3.2.3 Vertical displacement test*

Giving the VCM a 500-μm amplitude sinusoidal command signal, the vertical displacement is obtained by capacitive sensor shown in Fig. 6. It is noted that the amplitude of the vertical displacement is about 3.4 μm, greater than the calculated value of 2.1 μm. The main reason is that the rotation of the circular notch-type hinge is generated by the bending of the weakest link of the hinge, not an absolute rotation; there is still a compression and dislocation. So, the actual vertical displacement is slightly larger than the calculated values. Manufacturing errors of flexure hinges also make the actual result different from calculated value.

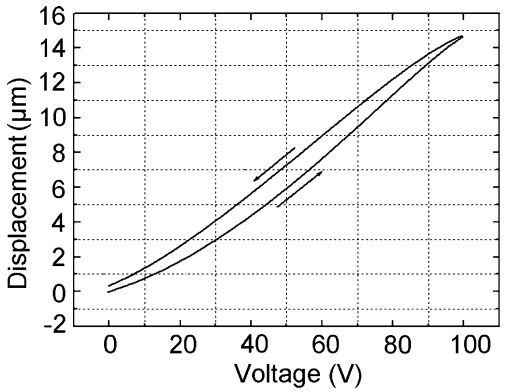


**Fig. 5** Hysteresis of the piezoelectric actuator actuated flexure structure under open-loop control

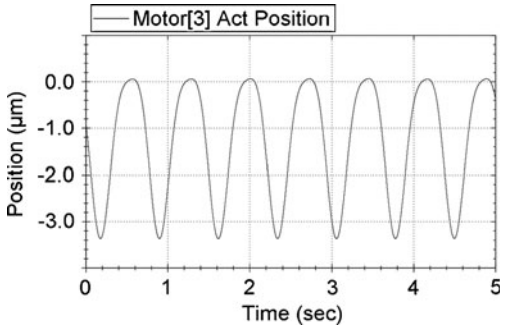


**Fig. 6** Vertical displacement of the long-stroke flexure structure

## 4 Closed-loop control experiments

For feedback control of this system, a simple PID controller $G_C(s)$ controller was implemented as:

$$G_C(s) = k_p + k_d s + \frac{k_i}{s} \tag{7}$$

where $k_p$, $k_d$, and $k_i$ are the proportional, derivative and integral gains. The performance of the small flexure hinge actuated by piezoelectric actuator and the big flexure hinge actuated by VCM were tested, respectively.

Under the closed-loop control, the performance of the flexure structure was improved obviously. Figure 7 shows the hysteresis phenomenon of the short-stroke flexure hinge under closed-loop control condition. The hysteresis phenomenon of the piezoelectric actuator was reduced, and the linearity of the flexure-based mechanism was improved.

Figure 8 shows the step responses of the two closed-loop controlled flexure hinges. The retraction process of the VCM actuated flexure hinge was also tested which was almost the same with the extension process. The overshoot of the two flexure hinges were eliminated by the PID controller, and the steady-state errors are both small enough. The rise time of the long-range FTS is 15 ms and the other is 12 ms.

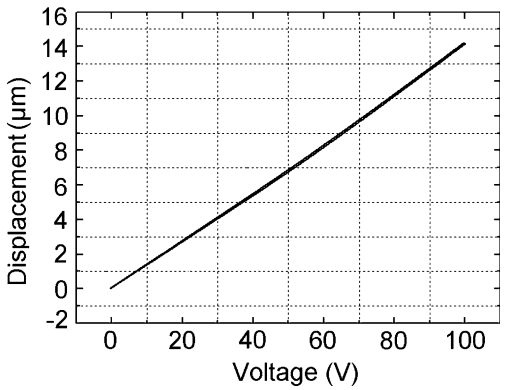


**Fig. 7** Hysteresis of the piezoelectric actuator actuated flexure structure under closed-loop control

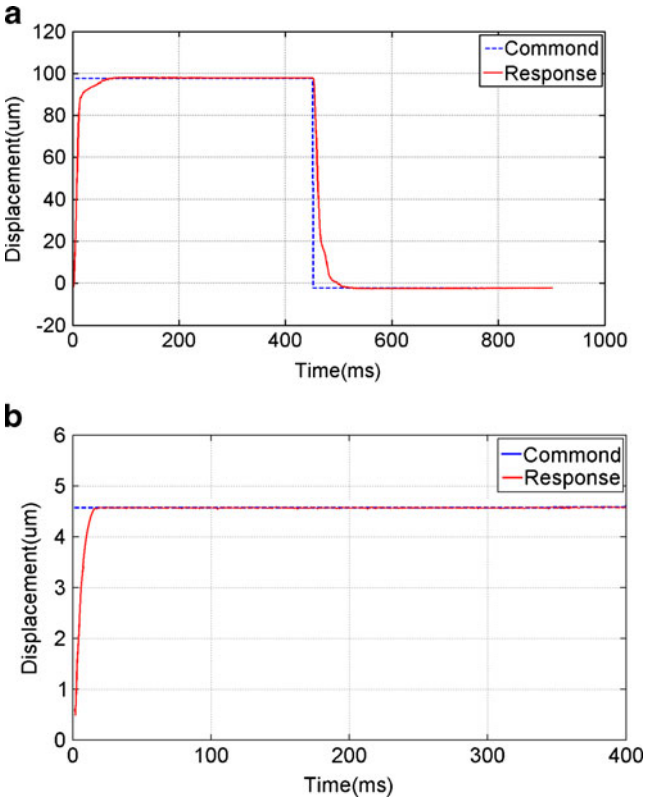


**Fig. 8** Step response of closed-loop control FTS: **a** tracking performance, **b** partial enlarged drawing

Under the closed-loop control condition, the tracking result of the VCM for a 400-μm amplitude sine wave input is illustrated in Fig. 9. The remaining maximum error of the long-stroke flexure hinge is about 0.6 μm which is about 0.15% of the full stroke. Also, a 4-μm sine wave signal was given to the piezoelectric actuator, and the result is shown in Fig. 10. The following error is about 0.013 μm. This remaining error is considered acceptable in this experiment.

In order to obtain the impact generated by the working short-stroke flexure on the long-stroke flexure hinge, a 10-Hz, 4-μm amplitude sinusoidal command signal was given to the piezoelectric actuator. The result showed that the impact on the tracking accuracy of the long-stroke flexure hinge can be ignored. In other words, the movements of the two flexure hinges are independent of each other in this application.

The resolution is one of the main targets of high precision positioning. Some factors such as environmental disturbance, error, and noises generated by equipment may reduce the resolution of the flexure-based mechanism. In order to examine the resolution of the flexure hinges, stair-control signals were applied to the amplifiers of the two actuators, and the displacements of the flexure hinges were recorded by a linear encoder and a capacitive sensor. The resolution was obtained as shown in Fig. 11. It can be seen

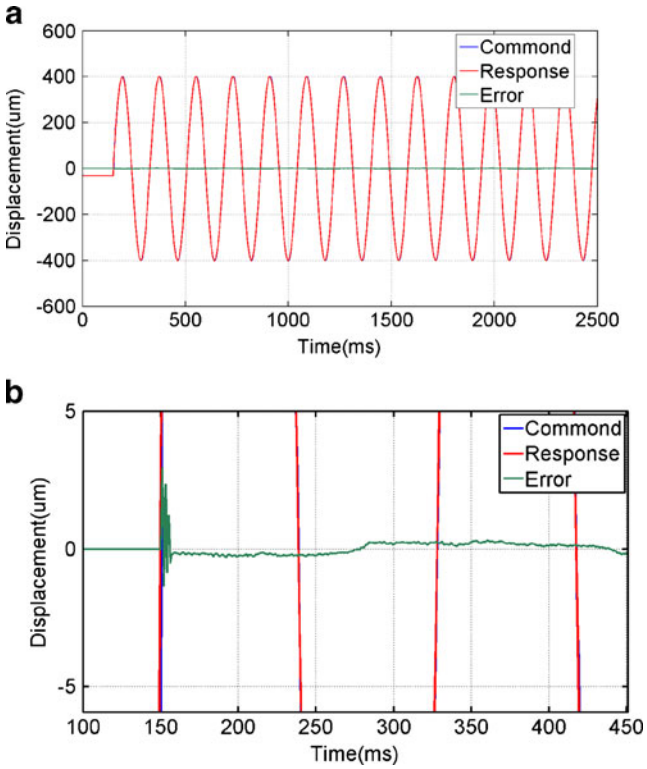


**Fig. 9** Tracking performance of long-stroke flexure structure: **a** tracking performance, **b** partial enlarged drawing

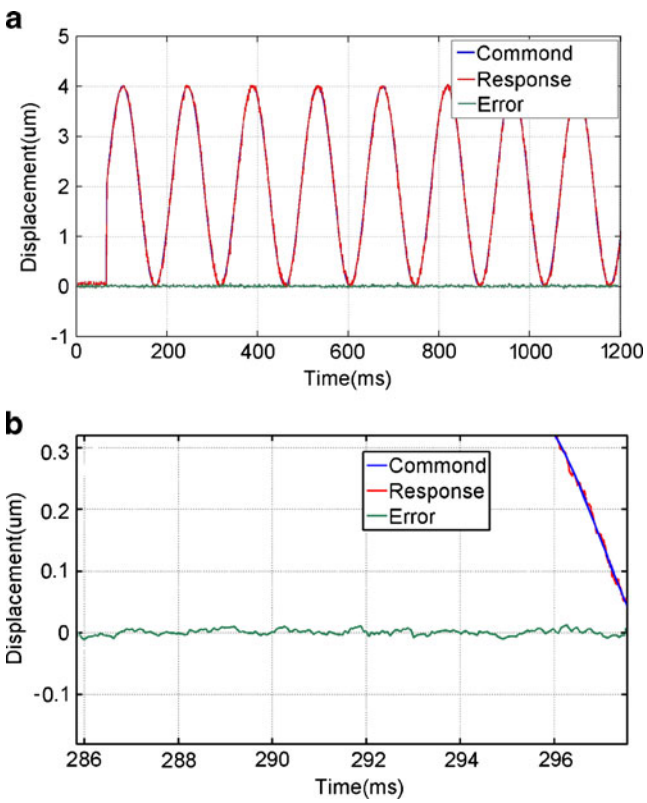


**Fig. 10** Tracking performance of short-stroke flexure structure: **a** tracking performance **b** partial enlarged drawing

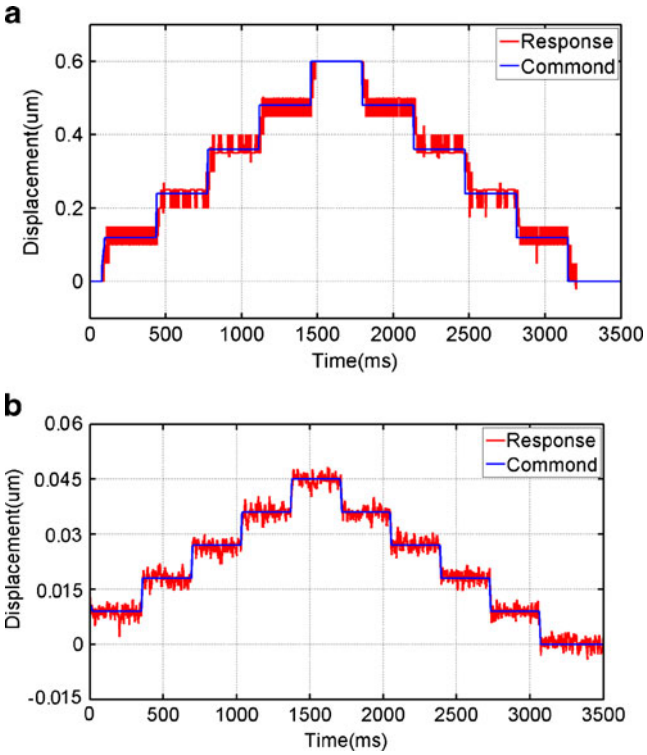


**Fig. 11** Resolution of the flexure structure under closed-loop control: **a** long stoke flexure structure **b** short stroke flexure structure

that the resolution of the long-stroke flexure hinge is 0.12 μm and that of the short-stroke flexure hinge is 9 nm. In fact, a high resolution can be obtained if the noise can be strictly controlled to a minimum level.

The movement of the tool is synthesized by the two flexure hinges' movements. The long-stroke flexure hinge driven by VCM provides the tool displacement in *z*-axis direction, and the piezoelectric actuator drives the short-stroke flexure hinge to offset the vertical displacement.

The capacitive sensor was fixed on the base of the FTS which measures any position changes of the tool in the *y*-axis direction. So, the short-stroke flexure hinge can compensate the vertical errors under closed-loop control

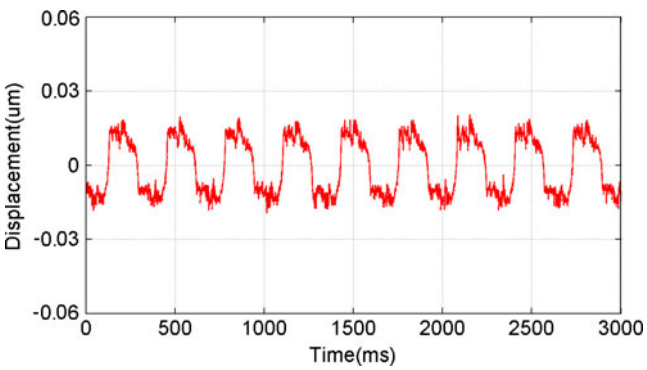


**Fig. 12** Vertical displacement of the tool

condition. A sinusoidal command signal was given to the VCM to examine the vertical error. The vertical displacement of the tool measured by another capacitive sensor is shown in Fig. 12. It can be seen that the displacement is about 0.022 μm. In this case, the short-stroke flexure hinge can compensate all of the errors in the *y*-axis direction.

## 5 Conclusion

Utilizing a VCM, a piezoelectric actuator, and two flexure hinges, a novel long-stroke FTS is developed. The long-stroke flexure hinge made the high-accuracy guide mechanism easy to machine. Actuated by VCM, the stroke of the FTS can reach up to ±0.5 mm, with a high resonance frequency in the *z*-axis direction which is approximately 109.6 Hz. The damping coefficient of this FTS is about 25.25 Ns/m. Besides, the short-stroke flexure hinge actuated by piezoelectric actuator can improve the closed-loop stiffness in *y*-axis direction. So, the FTS has high stiffness in *y*-axis direction and high resonance frequency in *z*-axis direction.

Controlled by PID controller, the FTS eliminated the overshoot of the two flexure hinges and obtained high response speed. The tracking error of the long-stroke flexure hinge actuated by VCM is 0.15%, and the short-stroke flexure hinge is about 0.013 μm. The vertical jump is 0.045 μm. So, the FTS system has a high tracking accuracy in the *z*-axis direction and high precision error compensation in the *y*-axis direction.

In sum, this long-stroke FTS has met the design requirements: utilizing the flexure hinge as the guide mechanism which made the long-stroke FTS easy to machine, high resonance frequency in *z*-axis direction, high stiffness in *y*-axis direction, and making the error compensation achievable in *y*-axis direction.

The FTS can obtain even long stroke by increasing the length of link $L_1$ and the other sizes of the circular notch-type hinges. The resolution and tracking accuracy of the FTS can be improved by the following aspects: better experimental environment and equipment to control the environment noise to a minimum level, a more precise control algorithm to control the FTS, triangle flexure hinge or other flexure hinges with better rotation capacity to replace circular notch-type hinges, and developing a better method to offset the inertia force which can make the FTS work at a higher frequency.

**Acknowledgment** The authors are grateful to the financial support from the National Science Foundation of China (50775099), the Ministry of Science and Technology of China (2008AA04Z125), the Ministry of Education of China (20070183104), and the Department of Science & Technology of Jilin Province, China (20080357; 20090337).

## References

1. Patterson SR, Magreb EB (1985) Design and testing of a fast tool servo for diamond turning. Precis Eng 7(3):123–128. doi:10.1016/0141-6359(85)90030-3
2. Ku S, Larsen G, Cetinkunt S (1998) Fast tool servo control for ultra-precision machining at extremely low feed rates. Mechatronics 8:381–393. doi:10.1016/S0957-4158(97)00063-9
3. Zhu W-H, Jun MB, Altintas Y (2001) A fast tool servo design for precision turning of shafts on conventional CNC lathes. Int J Mach Tool Manu 41(6):953–965. doi:10.1016/S0890-6955(00)00118-8
4. Gan S-W, Lim H-S, Rahman WF (2007) A fine tool servo system for global position error compensation for a miniature ultra-precision lathe. Int J Mach Tool Manu 47:1302–1310. doi:10.1016/j.ijmachtools.2006.08.023
5. Kim HS, Kim EJ (2003) Feed-forward control of fast tool servo for real-time correction of spindle error in diamond turning of flat surface. Int J Mach Tool Manu 43:1177–1183. doi:10.1016/S0890-6955(03)00156-1
6. Crudele M, Kurfess TR (2003) Implementation of a fast tool servowith repetitive control for diamond turning. Mechatronics 13:243–257. doi:10.1016/S0957-4158(01)00036-8
7. Ludwick SJ Jr (1999) A Rotary Fast Tool Servo for Diamond Turning of Asymmetric Optics. Dissertation, MIT
8. Brecher C, Lange S, Merz M, Niehaus F, Winterschladen M (2006) Off-axis machining of NURBS freeform surfaces by Fast Tool Servo Systems. In: Proceedings of the 4M 2006 Second International Conference on Multi-Material Micro Manufacture, Grenoble, France, pp 59–62. doi:10.1016/B978-008045263-0/50013-1
9. Lu XD (2005) Electromagnetically-Driven Ultra-Fast Tool Servos for Diamond Turning. Doctor Dissertation, MIT
10. Montesanti RC (2005) High Bandwideth Rotary Fast Tool Servo and a Hybrid Rotary/Linear Electricmagnetic Actuator. Dissertation, MIT
11. Buescher NP (2005) Live-Axis Turning. Dissertation, NCSU
12. Zhong ZW, Lin G (2006) Ultrasonic assisted turning of an aluminium-based metal matrix composite reinforced with SiC particles. Int J Adv Manuf Technol 27:1077–1081. doi:10.1007/s00170-004-2320-3
13. Sosnicki O, Pages A, Pacheco C, Malillard T (2010) Servo piezoelectric tool SPT400MML for the fast and precise machining of free forms. Int J Adv Manuf Technol. doi:10.1007/s00170-009-21-6
14. Ma H, Dejin Hu, Zhang K (2005) A fast tool feeding mechanism using piezoelectric actuators in noncircular turning. Int J Adv Manuf Technol. doi:10.1007/s00170-004-2168-6
15. Dan Wu, Chen K (2010) Chatter suppression in fast tool servo-assisted turning by spindle speed variation. Int J Mach Tool Manu 50(12):1038–1047. doi:10.1016/j.ijmachtools.2010.09.001
16. Kim Ho-Sang, Kim Sang-In, Lee Kwang-Il, Lee D-H, Bang Y-B, Lee Kyo-Il (2009) Development of a programmable vibration cutting tool for diamond turning of hardened mold steels. Int J Adv Manuf Technol 40:26–40. doi:10.1007/s00170-007-1311-6
17. http://www.kineticceramics.com/optics_fabrication_equipment.html. Accessed 26 June 2010
18. Kima Ho-Sang, Lee Kwang-Il, Lee K-M, Bang Y-B (2009) Fabrication of free-form surfaces using a long-stroke fast tool servo and corrective figuring with on-machine measurement. Int J Mach Tool Manu 49:991–997. doi:10.1016/j.ijmachtools.2009.06.011

19. Noh YJ, Nagashima M, Arai Y, Gao W (2009) Fast Positioning of Cutting Tool by a Voice Coil Actuator for Micro-Lens Fabrication. Int J of Automation Technology 3(3):257–262
20. Zdanowicz EM (2009) Design of a Fast Long Range Actuator-FLORA II. Dissertation, NCSU
21. Byl MF (2005) Design and Control of a Long Stroke Fast Tool Servo. Dissertation, MIT
22. http://www.precitech.com/2010_Precitech_FTS.html. Accessed 6 June 2010
23. http://www.nanotechsys.com/accessories/nanotech-250upl-factory-options. Accessed 22 June 2010
24. Rakuff S, Cuttino JF (2009) Design and testing of a long-range, precision fast tool servo system for diamond turning. Precis Eng 33(1):18–25. doi:10.1016/j.precisioneng.2008.03.001
25. Rakuff S (2004) Development of a precision long-range fast tool servo system for diamond turning. Dissertation, NCUC
26. Yin ZQ, Dai YF, Li SY, Guan CL, Tie GP (2010) Fabrication of off-axis aspheric surfaces using a slow slide tool servo. Int J Mach Tool Manu 51:404–410. doi:10.1016/j.ijmachtools.2011.01.008
27. Paros JM, Weisbord L (1965) How to design a flexure hinge. Mach Des 37:151–157